Journal of Current Science and Technology, May-August 2021 Vol. 11 No. 2, 334-341

ISSN 2630-0656 (Online)

Cite this article: Teerasuchai, K., Ksapabutr, B., Panapoy, M., & Chaiyut, N. (2021, May). Preparation and properties of poly(butylene succinate) porous scaffold by fused deposition modeling and salt leaching techniques. *Journal of Current Science and Technology, 11*(2), 334-341. DOI: 10.14456/jcst.2021.33

Journal of Current Science and Technology

Journal homepage: https://jcst.rsu.ac.th

Preparation and properties of poly(butylene succinate) porous scaffold by fused deposition modeling and salt leaching techniques

Kasidis Teerasuchai, Bussarin Ksapabutr, Manop Panapoy, and Nattawut Chaiyut*

Department of Materials Science and Engineering, Faculty of Engineering and Industrial Technology, Silpakorn University, Sanamchandra Palace Campus, Nakhon Pathom 73000, Thailand

*Corresponding author: E-mail: chaiyut_n@su.ac.th

Received 18 March 2021; Revised 24 April 2021; Accepted 12 May 2021;
Published online 27 May 2021

Abstract

Scaffolds are a promising innovation that create a suitable environment for the restoration of tissues. They can also be used to achieve efficient drug delivery to specific sites. Poly(butylene succinate) (PBS) is a biocompatible and biodegradable polymer that has been utilized in various research fields. Fused deposition modeling (FDM) was conducted to construct PBS scaffolds with two specific lay-down patterns: grid and triangle. The salt leaching technique was also used to produce pores in the scaffolds. A morphological study, porosity measurement, and contact angle analysis were carried out to characterize scaffold morphology, pore characteristics and surface properties. Salt content and type of lay-down patterns were found to affect the porosity and wettability of the scaffolds. Porosity increased with an increasing proportion of salt while scaffolds with a triangle pattern were more porous than grid pattern at the same salt content. The wettability test showed that the contact angle of all scaffolds ranged between 88° and 102°, while the grid pattern was more hydrophobic than the triangle pattern.

Keywords**:** *fused deposition modeling; poly(butylene succinate); porosity; porous scaffold; salt leaching; wettability.*

1. Introduction

Over the last few decades, scaffolds have been developed to deliver cultured cells or drugs to repair and restore infected tissue. Scaffold design should include suitable properties for use as a drug delivery system, such as being porous to increase the scaffold surface area, with various possible shapes. Drug delivery system can be a formula or device that can carry drugs or other substances directly to target areas in the body. The efficiency and safety of using drugs can be increased by controlling the release rate to reduce the total amount of drugs required for therapeutic effect (Biswas, Shukla, & Maiti, 2019).

Many factors control the absorption rate and release rate of drugs. One of the most important is the material properties used to create the scaffold. Some biopolymers including poly(lactic acid) (PLA), poly(glycolide) (PGA), poly(caprolactone) (PCL), and poly(beta-hydroxybutyrate) (PHB) have good biological compatibility. However, these polymers have disadvantages such as long biodegradation time or high raw material cost (Huang et al., 2018). Poly(butylene succinate) or PBS is a commercially available biodegradable polymer that can be efficiently synthesized through condensation polymerization from succinic acid and 1,4-butanediol. The properties of PBS are similar to conventional petroleum-based polymers such as polyethylene (Platnieks et al., 2020), while it also has good biodegradation and biocompatibility properties for tissue engineering applications. PBS was used as the material for a bimodal scaffold to promote cell growth (Ju et al., 2020), growth of mesenchymal stem cells (Ojansivu et al., 2018), and drug encapsulation

systems (Liu & Guo, 2019). With these advantages, PBS has received increasing attention regarding possible applications in tissue engineering and controlled drug delivery (Gigli et al., 2016).

In addition to the materials, the processing technique is another important factor affecting drug delivery efficiency and appropriate release times. The fused deposition modeling (FDM) technique is one of the most widely used additive manufacturing processes for fabricating prototypes and functional parts in various plastics (Hu, & Qin, 2020). It is also a powerful tool to create patient-specific porous scaffolds by modifying the input materials to adjust local drug delivery capability (Water et al., 2015). Choi et al. (2020) developed biocompatible PLA scaffolds fabricated by FDM and foam extrusion techniques for medical use. FDM was also used to produce lactose-crosslinked gelatin scaffolds as a drug delivery system for dexamethasone (Etxabide, Long, Guerrero, de la Caba, & Seyfoddin, 2019) and fabricate porous hydroxyapatite scaffolds for bone regeneration and local drug delivery applications (Mondal & Pal, 2019). Moreover, drug absorption and release rate were also shown to be controlled by the pore size and porosity of the materials (Saghazadeh et al., 2018). The particulate leaching technique is one of the simplest methods to produce pores in a material. Sodium chloride (NaCl) is the most common material using as a porogen for this technique. The size of NaCl particles controls the pore size, while the amount of NaCl controls the porosity. Obayemi et al. (2020) introduced polymer blends porous scaffolds using solvent casting and salt leaching for localized cancer drug delivery and breast cell/tissue growth, while Li et al. (2020) fabricated composite scaffolds for long-term controlled dual drug release via particle leaching combined with phase separation technique. Recently, Gorji et al. (2021) prepared a poly(lactide-co-glycolic acid) scaffold via the salt leaching method as a herbal drug-release application.

Combining FDM and particulate leaching techniques is a promising method for fabricating a porous scaffold for drug control release application, especially for a heat-sensitive drug, since this method ensures that the drug will not come into contact with heat during the fabrication and drug loading processes, and not be subjected to thermal degradation. Visscher, Dang, Knackstedt, Hutmacher and Tran (2018) used FDM and particulate leaching techniques to fabricate polycaprolactone scaffolds with dual macro-microporosity for local delivery of antibiotics. Phosphate buffered saline powder was used as a porogen. However, they did not focus on porogen concentration and pattern type on the properties of the scaffolds. To the best of our knowledge, the influence of geometrical structure on scaffold properties has not been reported elsewhere.

2. Objectives

1. To fabricate porous scaffolds by FDM and salt leaching techniques.
2. To study the effect of NaCl concentration on the morphology, porosity and wettability of the scaffolds.
3. To study the effect of type of lay-down patterns on the morphology, porosity and wettability of the scaffolds.

3. Materials and methods

3.1 Materials

PBS grade BioPBS™ FZ71PM was purchased from PTT MCC Biochem Co., Ltd. (Bangkok, Thailand). The density of PBS was 1.26 g/cm^3 and the melt flow index was 22 g/10 min (measured at 190°C, 2.16 kg). Analytical grade NaCl 99%, silver nitrate ($AgNO_3$) and dichloromethane (CH_2Cl_2) were purchased from RCI Labscan Ltd. (Bangkok, Thailand).

3.2 Fabrication of porous scaffold

NaCl was ground and sieved to obtain particle sizes in the range 38-75 μm. PBS sheets containing four different NaCl amounts (0, 40, 50 and 60 %wt) were prepared by the solvent casting method. Firstly, PBS pellets were dissolved in dichloromethane. When they were completely dissolved, NaCl at a certain weight ratio to PBS was added into the PBS solution. A mechanical stirrer was used to disperse the NaCl particles homogeneously and the suspension was poured into a glass mold. The mold was placed in a fume hood to evaporate the solvent completely. Cast sheets with specific weight ratios of NaCl were cut into small pieces and then molten mixed in a co-rotating twin-screw extruder to form extruded filaments.

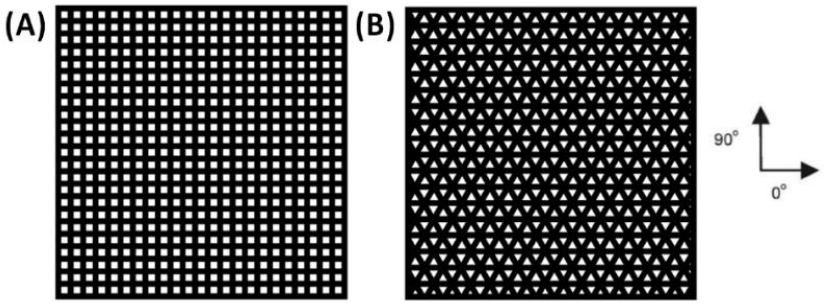

Figure 1 Schematic diagrams of (A) grid and (B) triangle lay-down patterns

The filament with a certain amount of NaCl was installed in a 3D-printing machine to construct the scaffold by FDM. Scaffolds with two lay-down patterns as; triangle and grid were fabricated, and schematic diagram patterns are shown in Figure 1. The infill of both scaffold patterns was fixed at 80%. The nozzle temperature of the 3D-printing machine was set at 190°C, while the dimensions of the constructed scaffold were 30 × 30 × 2 mm^3. The salt leaching technique was conducted to dissolve NaCl. Constructed scaffolds embedding different NaCl contents were immersed in deionized water. This process continued until NaCl completely dissolved. This was checked by adding a few drops of $AgNO_3$ solution into the leached deionized water and no trace of white AgCl precipitate was detected. The obtained scaffolds were then dried in an oven at 60 °C for 12 hours. A NaCl-generated porous scaffold was denoted as a NGP scaffold and a NaCl-free porous scaffold was denoted as a NFP scaffold. Table 1 lists the codename, polymer-to-salt ratio and lay-down patterns of the scaffolds studied in this research.

Table 1 Codename, polymer-to-salt ratio and lay-down patterns of the scaffolds

Codename	PBS:NaCl ratio (%wt)	Lay-down pattern
10:0PBS-g	100:0	Grid
10:0PBS-t	100:0	Triangle
6:4PBS-g	60:40	Grid
6:4PBS-t	60:40	Triangle
5:5PBS-g	50:50	Grid
5:5PBS-t	50:50	Triangle
4:6PBS-g	40:60	Grid
4:6PBS-t	40:60	Triangle

3.3 Morphological observations

A scanning electron microscope (SEM; TM3030 Hitachi, Japan) operating at 15 kV was used to observe scaffold morphology on the external fiber surface and the cryo-fractured internal surface. To examine the internal surface, the scaffold was immersed and cryo-fractured under liquid nitrogen, while the external surface observation did not require these preparation steps. The external and cryo-fractured internal surfaces were then coated with platinum using a sputtering coater operating at 20 mA under an argon atmosphere. Pore sizes in the SEM micrographs were measured with ImageJ (National Institutes of Health, USA).

3.4 Porosity measurement

Porosity of the scaffolds was calculated using a Density Determination Kit (Sartorius YDK03, Göttingen, Germany) assembled with an electronic balance. The scaffold was immersed in distilled water and its weight change was measured. Applying Archimedes principle, when the scaffold was immersed in a liquid it was subjected to a buoyant force with a value equal to the weight of the liquid displaced by the volume of the scaffold, denoted as weight in water ($W_{in\ water}$). The specific gravity (ρ) was calculated using equation (1):

$$\rho = \frac{W_{in\ air} * (\rho_{water} - \rho_a)}{(W_{in\ air} - W_{in\ water})} + \rho_a \qquad (1)$$

where $W_{in\ air}$ is the weight of the scaffold in air, $W_{in\ water}$ is the weight of the scaffold in water, ρ_{water} is the density of water (0.99707 g/cm^3 at 25 °C) and ρ_a is the density of air under standard conditions (0.00118 g/cm^3 at 25 °C) (Kumar, Haldar, Rajesh, Ghosh, & Lahiri, 2019).

Percentage of porosity of the scaffold was calculated using equation (2):

$$\%\text{porosity} = \frac{\rho - \rho_{bulk}}{\rho} * 100 \qquad (2)$$

where ρ_{bulk} is the bulk density of the scaffold. The bulk density was determined from the weight in air and the volume of the scaffold.

3.5 Contact angle analysis

The contact angle of the scaffold was examined using a USB digital microscope (DigiMicro Profi, DNT) attached to an Axis Feed Auger Stage (RM-XYZ, MiSUMi, Illinois, USA). Distilled water was used as the testing liquid.

4. Results and discussion

4.1 Scaffold morphological study

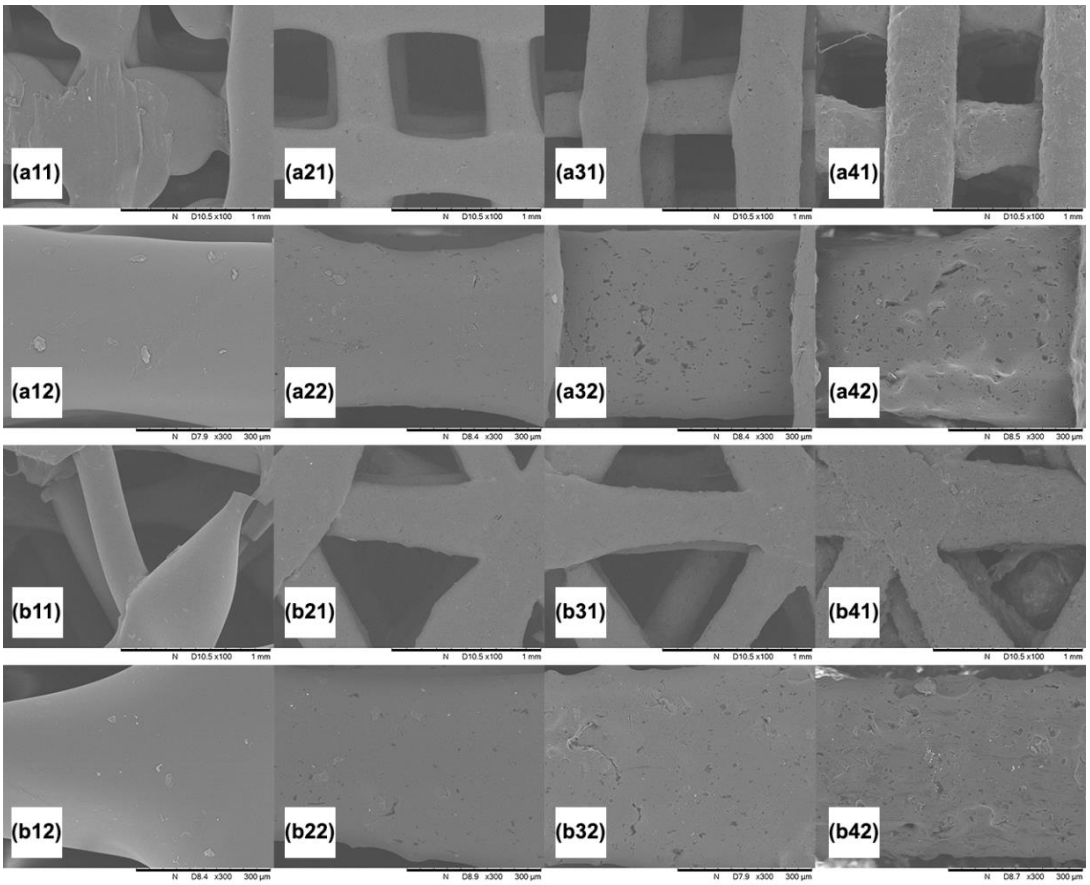

Figure 2 SEM images of the external surface morphology of (a) grid lay-down patterns of 10:0PBS-g (a11-a12), 6:4PBS-g (a21-a22), 5:5PBS-g (a31-a32) and 4:6PBS-g (a41-a42), and (b) triangle lay-down patterns of 10:0PBS-t (b11-b12), 6:4PBS-t (b21-b22), 5:5PBS-t (b31-b32) and 4:6PBS-t (b41-b42). Images in rows 1 and 3 are at magnification 100x, with those in rows 2 and 4 at 300x

Figure 2 shows the external surface morphology of NFP and NGP scaffolds having different salt contents and lay-down patterns. The geometries of the grid and triangle lay-down patterns are shown in Figure 2 (rows 1 and 2) and Figure 2 (rows 3 and 4), respectively. The shapes of 3D printed fibers of the NFP scaffolds shown in Figure 2 column 1 were less stable to maintain fibrous shape than the NGP scaffolds, possibly due to the viscosity effect of the molten filament during processing. The NFP scaffolds exhibited relatively smoother fibrous surfaces than the NGP scaffolds. When the amount of salt increased from 40-60 %wt (Figure 2 columns 2-4), the surfaces of these NGP scaffolds became rougher, the number of pores increased and pore size was larger. However, there was no effect of the lay-down pattern on the fibrous surface morphology of the scaffolds containing different salt contents.

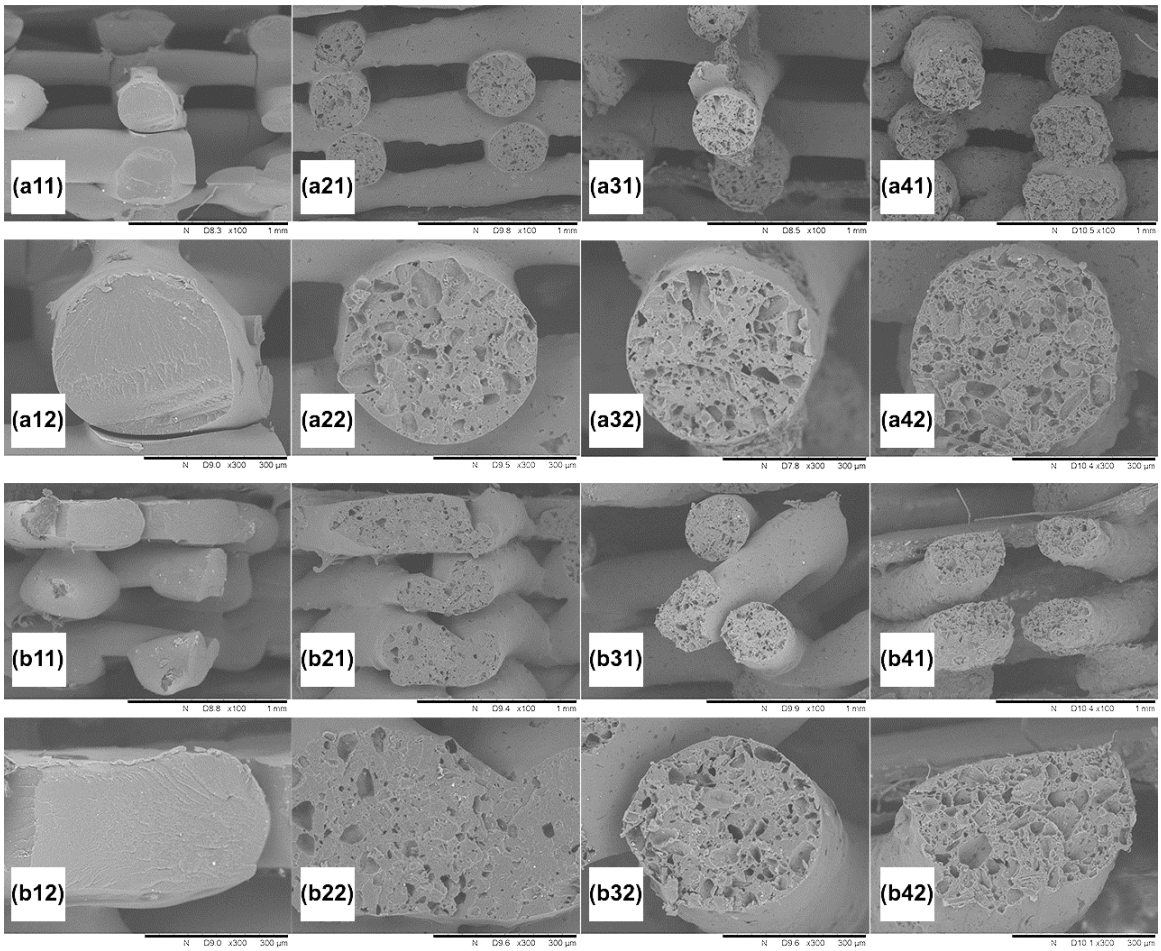

Figure 3 SEM images of the cryo-fractured surface morphology of (a) grid lay-down patterns of 10:0PBS-g (a11-a12), 6:4PBS-g (a21-a22), 5:5PBS-g (a31-a32) and 4:6PBS-g (a41-a42), and (b) triangle lay-down patterns of 10:0PBS-t (b11-b12), 6:4PBS-t (b21-b22), 5:5PBS-t (b31-b32) and 4:6PBS-t (b41-b42). Images in rows 1 and 3 are at magnification 100x, with those in rows 2 and 4 at 300x

The SEM images of the cryo-fractured NFP and NGP scaffolds having different amounts of salt and lay-down patterns are shown in Figure 3. The morphology of the NFP scaffolds (Figure 3 column 1) and NGP scaffolds (Figure 3 columns 2-4) displayed the same fashion as those on the fibrous surfaces. The NaCl particles dispersed well in the polymer matrix. For the NGP scaffolds, size of pores generated by salt leaching in the matrix was measured and listed in Table 2. Their size ranged from 3.77-49.39 µm, while no internal pores were observed in the NFP scaffolds. Internal pore size increased at higher salt content indicating an agglomeration of salt particles in the scaffold matrix. The agglomeration became more obvious with addition of more salt. However, the type of lay-down pattern did not influence the internal pore size of the scaffolds. The SEM micrographs in Figures 2 and 3 showed that salt particles tended to be confined to the scaffold's internal matrix rather than on the external surface. With increasing amount of salt, Figure 2 showed that higher amount of salt particles was exposed on the surface, while Figure 3 showed that salt particles were mainly embedded in the matrix. This might be due to the difference between the scaffold's internal volume that was significantly greater than the scaffold's external surface area. Moreover, interconnected pores became more developed, thus enhancing the efficiency of the encapsulation and control release properties with increasing salt content (Zhang, Fan, Dunne, & Li, 2018). Although the scaffolds

contained different amounts of salt, the lay-down patterns did not affect the cryo-fractured morphology of the scaffolds.

4.1 Porosity of the scaffolds

The porosity of a scaffold represents the void space within it. The porosity values of all scaffolds, calculated by the specific gravity determination method, are shown in Figure 4A and summarized in Table 2. The NFP scaffolds with grid and triangle lay-down patterns exhibited 38.12% and 40.05% porosity, respectively, which showed that the triangle pattern occupied a higher void space than the grid pattern. All the NGP scaffolds displayed greater porosity than the NFP scaffolds due to the dissolution of NaCl during the salt leaching process. The porosity was directly related to the salt content; the higher the salt content, the greater the porosity. Moreover, porosity of the triangle pattern was higher than the grid one, and the difference between these two patterns was more pronounced when salt content increased. This occurred because theoretically, at fixed 80% infill, the triangle lay-down pattern consumed more PBS/NaCl filament to fabricate the scaffold than the grid pattern. Therefore, the triangle occupied greater porosity.

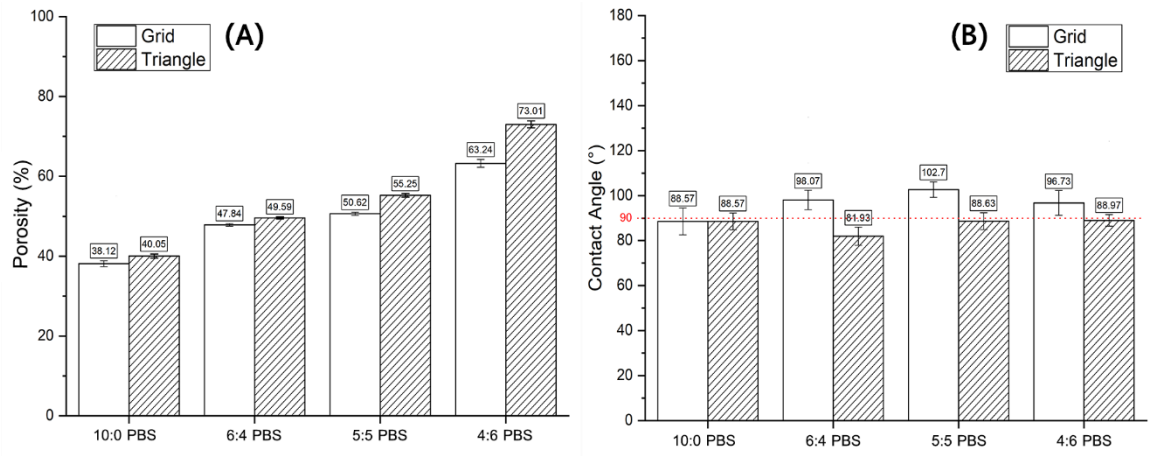

Figure 4 (A) Percentage of porosity and (B) contact angle measurement of the NFP and NGP scaffolds with different lay-down patterns. Horizontal red dashed lines indicate the threshold contact angle of 90° between hydrophobic and hydrophilic properties

Table 2 Porosity, internal pores size and contact angle of the scaffolds

Sample	Porosity (%)	Internal pores size (μm)	Contact angle (°)
10:0PBS-g	38.12±0.73	-	88.57±5.96
6:4PBS-g	47.84±0.35	3.77 – 25.06	98.07±4.26
5:5PBS-g	50.62±0.37	5.06 – 37.51	102.70±3.42
4:6PBS-g	63.24±0.97	6.88 – 49.61	96.73±5.51
10:0PBS-t	40.05±0.50	-	88.57±3.73
6:4PBS-t	49.59±0.29	3.89 – 27.70	81.93±4.05
5:5PBS-t	55.25±0.44	4.74 – 36.33	88.63±3.77
4:6PBS-t	73.01±0.89	7.12 – 48.39	88.97±2.58

4.2 Wettability of the porous scaffolds

The contact angle testing results of the NFP and NGP scaffolds with different lay-down patterns are shown in Figure 4B and tabulated in Table 2. The NFP scaffolds had the same contact angle of 88.57°, which was close to a neutral value of 90° regardless of the lay-down pattern. When higher salt content was added to the scaffold, porosity increased and larger pore sizes were obtained. Scaffolds with the grid lay-down pattern exhibited an increase in contact angle from 88.57° for 10:0PBS-g to 98.07° and 102.70° for 6:4PBS-g and 5:5PBS-g, respectively, and then

decreased to 96.73° for 4:6-PBS-g. This indicated that porous scaffolds with the grid pattern became more hydrophobic with increasing salt content. By contrast, porous scaffolds with the triangle pattern displayed almost the same contact angle regardless of salt content; thus, the scaffolds still displayed hydrophilic behavior. This might be due to the surface roughness caused by the small pores left by leaching of salt particles and air trapped on the scaffold's surface, resulting in higher hydrophobicity of the grid pattern, concerning with Senthamizhan, Balusamy, Celebioglu, and Uyar (2016) and Szewczyk et al. (2019). Wettability is one of the factors use to determine the usability of scaffolds as drug release control. The human body comprises 66% water and the porous scaffold should behave as a hydrophilic material to ease the release of an absorbed drug by water in the body. Thus, the 4:6PBS-t porous scaffold having the triangle pattern, highest porosity and largest pore size was chosen for further testing in drug delivery application.

5. Conclusions

Porous scaffolds of PBS were successfully fabricated by FDM and salt leaching techniques. The leaching process successfully created a large number of pores (porosity) in the NGP scaffolds with various pore sizes depending on the amount of salt and also on the type of lay-down patterns. The porosity of the NGP scaffolds increased with an increasing proportion of salt. Contact angle measurement indicated that the NFP scaffolds showed no difference in contact angle between the two lay-down patterns; however, the NGP scaffolds with the grid pattern were more hydrophobic than the triangle pattern. Scaffolds with suitable porosity, pore size as well as wettability perform better for drug release control.

6. Acknowledgements

The authors would like to gratefully thank the Department of Materials Science and Engineering, Faculty of Engineering and Industrial Technology, Silpakorn University, Thailand, for financial supports.

7. References

Biswas, A., Shukla, A., & Maiti, P. (2019). Biomaterials for interfacing cell imaging and drug delivery: An overview. *Langmuir*, *35*(38), 12285-12305. DOI: https://doi.org/10.1021/acs.langmuir.9b00419

Choi, W. J., Hwang, K. S., Kwon, H. J., Lee, C., Kim, C. H., Kim, T. H., ... & Lee, J. Y. (2020). Rapid development of dual porous poly (lactic acid) foam using fused deposition modeling (FDM) 3D printing for medical scaffold application. *Materials Science and Engineering: C*, *110*, 110693. DOI: https://doi.org/10.1016/j.msec.2020.110693

Etxabide, A., Long, J., Guerrero, P., de la Caba, K., & Seyfoddin, A. (2019). 3D printed lactose-crosslinked gelatin scaffolds as a drug delivery system for dexamethasone. *European Polymer Journal*, *114*, 90-97. DOI: https://doi.org/10.1016/j.eurpolymj.2019.02.019

Gigli, M., Fabbri, M., Lotti, N., Gamberini, R., Rimini, B., & Munari, A. (2016). Poly(butylene succinate)-based polyesters for biomedical applications: A review. *European Polymer Journal*, *75*, 431-460. DOI: https://doi.org/10.1016/j.eurpolymj.2016.01.016

Gorji, M., Zargar, A., Setayeshmehr, M., Ghasemi, N., Soleimani, M., Kazemi, M., & Hashemibeni, B. (2021). Releasing and structural/mechanical properties of nano-particle/Punica granatum (Pomegranate) in poly (lactic-co-glycolic) acid/fibrin as nano-composite scaffold. *Bratislavske Lekarske Listy*, *122*(1), 54-64. DOI: https://doi.org/10.4149/bll_2021_007

Hu, C., & Qin, Q. H. (2020). Advances in fused deposition modeling of discontinuous fiber/polymer composites. *Current Opinion in Solid State and Materials Science*, *24*(5), 100867. DOI: https://doi.org/10.1016/j.cossms.2020.100867

Huang, A., Peng, X., Geng, L., Zhang, L., Huang, K., Chen, B., ... & Kuang, T. (2018). Electrospun poly (butylene succinate)/cellulose nanocrystals bio-nanocomposite scaffolds for tissue engineering: Preparation, characterization and in vitro evaluation. *Polymer Testing*, *71*, 101-109. DOI: https://doi.org/10.1016/j.polymertesting.2018.08.027

Ju, J., Gu, Z., Liu, X., Zhang, S., Peng, X., & Kuang, T. (2020). Fabrication of bimodal open-porous poly (butylene succinate)/cellulose

nanocrystals composite scaffolds for tissue engineering application. *International Journal of Biological Macromolecules*, *147*, 1164-1173. DOI: https://doi.org/10.1016/j.ijbiomac.2019.10.085

Kumar, R. M., Haldar, S., Rajesh, K., Ghosh, S., & Lahiri, D. (2019). Comparative study on the efficacy of the UHMWPE surface modification by chemical etching and electrostatic spraying method for drug release by orthopedic implants. *Materials Science and Engineering: C*, *105*, 110117. DOI: https://doi.org/10.1016/j.msec.2019.110117

Li, D., Li, C., Wang, X., Li, C., Sun, T., Zhou, J., & Li, G. (2020). Facile fabrication of composite scaffolds for long-term controlled dual drug release. *Advances in Polymer Technology*, *2020*, 10. DOI: https://doi.org/10.1155/2020/3927860

Liu, Y., & Guo, B. (2019). Preparation and characterisation of poly (butylene succinate) microcarriers containing pesticide. *Micro & Nano Letters*, *14*(1), 81-85. DOI: https://doi.org/10.1049/mnl.2018.5060

Mondal, S., & Pal, U. (2019). 3D hydroxyapatite scaffold for bone regeneration and local drug delivery applications. *Journal of Drug Delivery Science and Technology*, *53*, 101131. DOI: https://doi.org/10.1016/j.jddst.2019.101131

Obayemi, J. D., Jusu, S. M., Salifu, A. A., Ghahremani, S., Tadesse, M., Uzonwanne, V. O., & Soboyejo, W. O. (2020). Degradable porous drug-loaded polymer scaffolds for localized cancer drug delivery and breast cell/tissue growth. *Materials Science and Engineering: C*, *112*, 110794. DOI: https://doi.org/10.1016/j.msec.2020.110794

Ojansivu, M., Johansson, L., Vanhatupa, S., Tamminen, I., Hannula, M., Hyttinen, J., ... & Miettinen, S. (2018). Knitted 3D scaffolds of polybutylene succinate support human mesenchymal stem cell growth and osteogenesis. *Stem cells international*, *2018*. 11. DOI: https://doi.org/10.1155/2018/5928935

Platnieks, O., Gaidukovs, S., Barkane, A., Sereda, A., Gaidukova, G., Grase, L., ... & Laka, M. (2020). Bio-based poly (butylene succinate)/microcrystalline cellulose/nanofibrillated cellulose-based sustainable polymer composites: Thermo-mechanical and biodegradation studies. *Polymers*, *12*(7), 1472. DOI: https://doi.org/10.3390/polym12071472

Saghazadeh, S., Rinoldi, C., Schot, M., Kashaf, S. S., Sharifi, F., Jalilian, E., ... & Khademhosseini, A. (2018). Drug delivery systems and materials for wound healing applications. *Advanced drug delivery reviews*, *127*, 138-166. DOI: https://doi.org/10.1016/j.addr.2018.04.008.

Senthamizhan, A., Balusamy, B., Celebioglu, A., & Uyar, T. (2016). "Nanotraps" in porous electrospun fibers for effective removal of lead (II) in water. *Journal of Materials Chemistry A*, *4*(7), 2484-2493. DOI: https://doi.org/10.1039/C5TA09166G

Szewczyk, P. K., Ura, D. P., Metwally, S., Knapczyk-Korczak, J., Gajek, M., Marzec, M. M., ... & Stachewicz, U. (2019). Roughness and fiber fraction dominated wetting of electrospun fiber-based porous meshes. *Polymers*, *11*(1), 34. DOI: https://doi.org/10.3390/polym11010034

Visscher, L. E., Dang, H. P., Knackstedt, M. A., Hutmacher, D. W., & Tran, P. A. (2018) 3D printed Polycaprolactone scaffolds with dual macro-microporosity for applications in local delivery of antibiotics. *Materials Science & Engineering C*, *87*, 78-89. DOI: https://doi.org/10.1016/j.msec.2018.02.008

Water, J. J., Bohr, A., Boetker, J., Aho, J., Sandler, N., Nielsen, H. M., & Rantanen, J. (2015). Three-dimensional printing of drug-eluting implants: preparation of an antimicrobial polylactide feedstock material. *Journal of pharmaceutical sciences*, *104*(3), 1099-1107. DOI: https://doi.org/10.1002/jps.24305

Zhang, K., Fan, Y., Dunne, N., & Li, X. (2018). Effect of microporosity on scaffolds for bone tissue engineering. *Regenerative biomaterials*, *5*(2), 115-124. DOI: https://doi.org/10.1093/rb/rby